16. Brunink, J. A. J. *et al.* The application of metalloporphyrins as coating material for quartz microbalance-based chemical sensors. *Anal. Chim. Acta* **325,** 53–64 (1996).
17. Di Natale, C. *et al.* The exploitation of metalloporphyrins as chemically interactive material in chemical sensors. *Mater. Sci. Eng. C* **5,** 209–215 (1998).
18. Blauer, G. & Sund, H. (eds) *Optical Properties and Structure of Tetrapyrroles* (de Gruyter, Berlin, 1985).
19. Nappa, M. & Valentine, J. S. The influence of axial ligands on metalloporphyrin visible absorption spectra. Complexes of tetraphenylporphinatozinc. *J. Am. Chem. Soc.* **100,** 5075–5080 (1978).
20. Suslick, K. S. & Van Deusen-Jeffries, S. in *Comprehensive Supramolecular Chemistry* (ed. Lehn, J. M.) 141–170 (Elsevier, Oxford, 1996).
21. Bhyrappa, P., Young, J. K., Moore, J. S. & Suslick, K. S. Dendrimer porphyrins: synthesis and catalysis. *J. Am. Chem. Soc.* **118,** 5708–5711 (1996).
22. Chou, J.-H., Nalwa, H. S., Kosal, M. E., Rakow, N. A. & Suslick, K. S. in *The Porphyrin Handbook* (eds Kadish, K., Smith, K. & Guilard, R.) 43–132 (Academic, New York, 2000).
23. Bhyrappa, P., Vaijayanthimala, G. & Suslick, K. S. Shape-selective ligation to dendrimer-metallo-porphyrins. *J. Am. Chem. Soc.* **121,** 262–263 (1999).
24. Sen, A. & Suslick, K. S. Shape selective discrimination of small organic molecules. *J. Am. Chem. Soc.* (in the press).
25. Adler, A. D. *et al.* A simplified synthesis for meso-tetraphenylporphin. *J. Org. Chem.* **32,** 476 (1967).
26. Adler, A. D., Longo, F. R., Kampas, F. & Kim, J. On the preparation of metalloporphyrins. *J. Inorg. Nucl. Chem.* **32,** 2443–2445 (1970).
27. Barley, M., Becker, J. Y., Domazetis, G., Dolphin, D. & James, B. R. Synthesis and redox chemistry of octaethylporphyrin complexes of ruthenium(II) and ruthenium(III). *Can. J. Chem.* **61,** 2389–2396 (1983).
28. Datta-Gupta, N. & Bardos, T. J. Synthetic porphyrins II: preparation and spectra of some metal chelates of para-substituted-meso-tetraphenylporphines. *J. Pharm. Sci.* **57,** 300–304 (1968).
29. Yaws, C. L. *Handbook of Vapor Pressure* (Gulf, Houston, 1994).

Supplementary Information is available on *Nature*'s World-Wide Web site (http://www.nature.com) or as paper copy from the London editorial office of *Nature*.

Acknowledgements

This work was supported by the US NIH and in part by the US DOD and DOE.

Correspondence and requests for materials should be addressed to K.S.S. (e-mail: ksuslick@uiuc.edu).

Timing of the Last Glacial Maximum from observed sea-level minima

Yusuke Yokoyama*†, Kurt Lambeck*, Patrick De Deckker‡, Paul Johnston* & L. Keith Fifield§

* *Research School of Earth Sciences,* ‡ *Department of Geology,* § *Department of Nuclear Physics, Research School of Physical Sciences and Engineering, The Australian National University, Canberra, ACT 0200, Australia*

During the Last Glacial Maximum, ice sheets covered large areas in northern latitudes and global temperatures were significantly lower than today. But few direct estimates exist of the volume of the ice sheets, or the timing and rates of change during their advance and retreat[1,2]. Here we analyse four distinct sediment facies in the shallow, tectonically stable Bonaparte Gulf, Australia—each of which is characteristic of a distinct range in sea level—to estimate the maximum volume of land-based ice during the last glaciation and the timing of the initial melting phase. We use faunal assemblages and preservation status of the sediments to distinguish open marine, shallow marine, marginal marine and brackish conditions, and estimate the timing and the mass of the ice sheets using radiocarbon dating and glacio-hydro-isostatic modelling. Our results indicate that from at least 22,000 to 19,000 (calendar) years before present, land-based ice volume was at its maximum, exceeding today's grounded ice sheets by 52.5×10^6 km^3. A rapid decrease in ice volume by about 10% within a few hundred years terminated the Last Glacial Maximum at 19,000 ± 250 years.

† Present address: Space Sciences Laboratory, University of California, Berkeley, California, USA, and Lawrence Livermore National Laboratory, 7000 East Avenue, PO Box 808, L-202 Livermore, California 94550, USA.

The broad and shallow continental margin of northern Australia includes several local bathymetric depressions, the largest of which is the Bonaparte Gulf. During times of sea-level lowstands much of the shelf was exposed, and the sediments deposited in the depressions were protected from wave action by the outer shelf edge. A total of 23 gravity cores, 10 vibrocores and 3 grab samples were collected from present-day water depths of 34 to 147 m along transects across the shelf margin and the Bonaparte depression (Fig. 1a). All cores were sedimentologically examined and a number were selected for micro-palaeontological analysis and radiocarbon dating. Depending on faunal assemblages and preservation status (Fig. 1b, see also Methods section below) four distinct bio-sedimentary facies have been recognized: open marine, shallow marine, marginal marine, and brackish water, denoted by OM, SM, MM and BR, respectively, in Fig. 1b. We obtained 41 radiocarbon dates of foraminifera and bivalve molluscs using accelerator mass spectrometry (AMS) techniques and dated some of the larger bivalves using conventional liquid scintillation counting methods. All AMS-dated samples were severely etched (about 40% to 50%) to discard outer shell material that may have been contaminated by secondary carbonate precipitation. Figure 1b summarizes the results for 7 of the cores from water depths between 128 and 95 m. All carbonate ages have been corrected for reservoir effect (400 years; refs 3, 4) and calibrated to a calendar timescale[5,6]. The cores indicate excellent preservation of faunal specimens, many without evidence for reworking, and the ^{14}C dates indicate only rare instances of age inversions.

Last Glacial Maximum (LGM) sea-level indicators are preserved in a number of the cores. To reconstruct a sea-level curve based on micropalaeontological evidence, it is necessary to consider the palaeoenvironmental conditions as a sequence of events assuming that little or no break in sedimentation, and no erosion, has occurred. (If a hiatus does occur it results in missing bio-facies and in reworking of the faunas; and this is not observed.) Thus, through identification of a transition from shallow marginal marine to brackish conditions and then back to shallow marginal marine conditions, the timing of the brackish conditions records the interval of lowest sea level. Once this depth is identified in a single core, other cores with depths either side of the identified low sea-level stand are examined to substantiate the reconstruction. This has been done using core GC5 as the master core because it has the best preserved and dated record for brackish water conditions. No truly lacustrine phase has been recognised in any of the cores, indicating that throughout the LGM the Bonaparte depression remained in open contact with the Timor Sea[7].

The transition from marginal marine to brackish facies occurs in core GC5 at 21,280 calendar years before present (cal. yr BP) at a depth of 340 cm below the sea floor (Fig. 1b). Sediments below this depth contain marine ostracods and planktonic foraminifers, whereas above this boundary dwarf specimens of the benthic foraminifer *Ammonia beccarii* occur along with other shallow to brackish water indicators such as the benthic foraminifer *Elphidium* spp. and the euryhaline ostracod *Cyprideis australiensis*[8,9]. Marginal marine and brackish-water conditions existed for about 3,000 years, in agreement with results from cores GC4 and GC6 (Fig. 1b) as well as GB1. Sea level at GC5 was, therefore, a few metres below −121 m (Fig. 2a) in this time interval. Deeper cores, both within the depression (GC1, GC2 and GC3) and outside it, do not indicate any brackish facies and place a lower limit of −125 m on the position of relative sea-level at these locations. The microfossil assemblages of cores GC10 and GC11, at −103 and −101 m respectively, are indicative of a marginal beach or coastal lagoon environment between 17,650 and 17,450 cal. yr BP. In core GC7, undamaged littoral-dwelling bivalves occur at −107 m with an age of 17,610 cal. yr BP (Fig. 1b). Figure 2a illustrates the results for all samples free from post-depositional disturbance. They indicate that between 22,000 and 19,000 cal. yr BP a rapid rise of 10–15 m occurred.

© 2000 Macmillan Magazines Ltd

The sea-level change due to the melting of land-based ice sheets is[10,11]

$$\Delta\zeta_{rsl} = \Delta\zeta_e + \Delta\zeta_i \quad (1)$$

where

$$\Delta\zeta_e(t) = -\frac{\rho_i}{\rho_w}\int_t \frac{1}{A_w(t)}\frac{dV_i}{dt}dt \quad (2)$$

is a measure of the ice volume V_i that contributed to the sea-level rise. We call this the ice-equivalent sea-level change. A_w is the ocean area and ρ_i, ρ_w are the average densities of ice and ocean, respectively. $\Delta\zeta_i$ is the total glacio-hydro-isostatic contribution to sea-level change. At the Australian sites, away from the former ice sheets, the isostatic response is one of subsidence of the sea floor and coastal zone because of the meltwater loading of the ocean floor. Here, $\Delta\zeta_i$ is

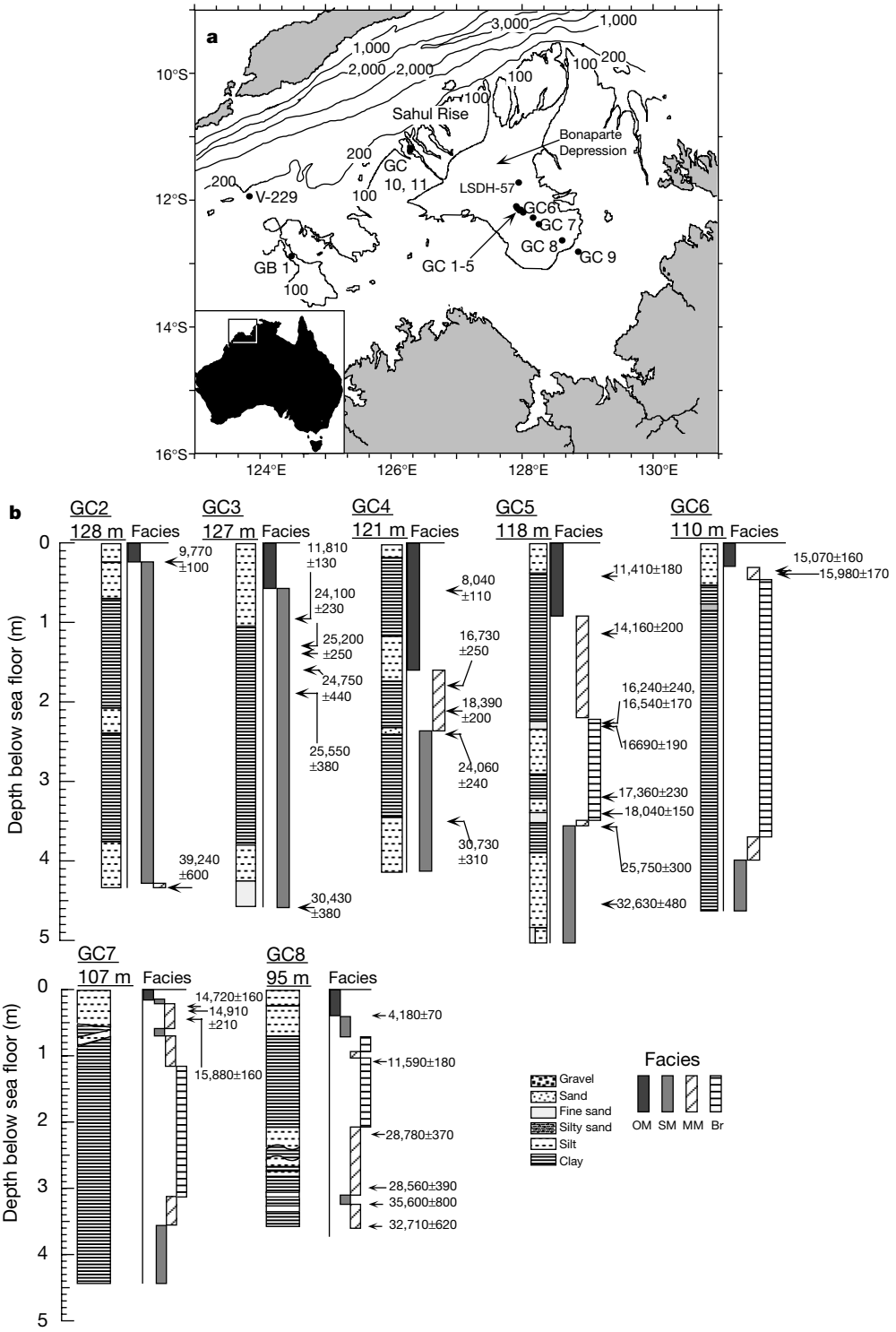

Figure 1 Location and stratigraphy of the Bonaparte cores. **a**, Location of the sampling sites on the northwest shelf of Australia with bathymetric contours (in metres) and coring sites. **b**, Sedimentological description with facies inferred from micro-palaeontological methods (see Methods) and ^{14}C dates for gravity cores. Four facies are identified as follows: OM, open marine; SM, shallow marine; MM, marginal marine; and BR, brackish-water (see Methods section). Dated horizons are indicated and all ages are in ^{14}C years. The complete data set, including calibrated ages, is available from http://www.ngdc.noaa.gov/paleo/data.html.

© 2000 Macmillan Magazines Ltd

about 10% of the primary contribution $\Delta\zeta_e$ and the relative sea levels lie above the ice-equivalent sea level at the time of the LGM[12].

The isostatic effects also need to be considered when estimating ice volumes from eustatic sea level $\Delta\zeta_{eus}$, defined as the globally averaged sea-level change. The value of $\Delta\zeta_i$ in equation (1) averaged over the oceans, $\langle\Delta\zeta_i\rangle_{Aw}$, at any time is non-zero because of the change in shape and depth of the ocean basin under the changing surface ice and water load. Hence the spatially averaged change in sea level at any time is $\Delta\zeta_{eus} = \Delta\zeta_e + \langle\Delta\zeta_i\rangle_{Aw}$ and the last term contributes about 20% to $\Delta\zeta_{eus}$. In addition to the time dependence of the depth of the ocean basin, the evaluation of the isostatic term in equation (1) and the integral in equation (2) includes the time dependence of both the coastline and the area of shallow sea floor covered by grounded ice.

Figure 2b illustrates the ice-equivalent sea level and associated land-based ice volume, inferred from the Bonaparte Gulf observations. These results use a rigorous glacio-hydro-isostatic formulation with Northern Hemisphere ice models that are consistent with observational evidence from these localities and with an Antarctic ice model that contributes 25 m to $\Delta\zeta_e$ (refs 13–15). Earth model parameters used in these corrections are based on analysis of Australian postglacial sea levels[12] and uncertainties in these parameters are included in evaluating the error bars of Fig. 2b. Because the isostatic corrections are about 10% of the total sea-level change, uncertainties in the distribution of ice between the different centres of glaciation contribute little to the magnitude of the isostatic effects

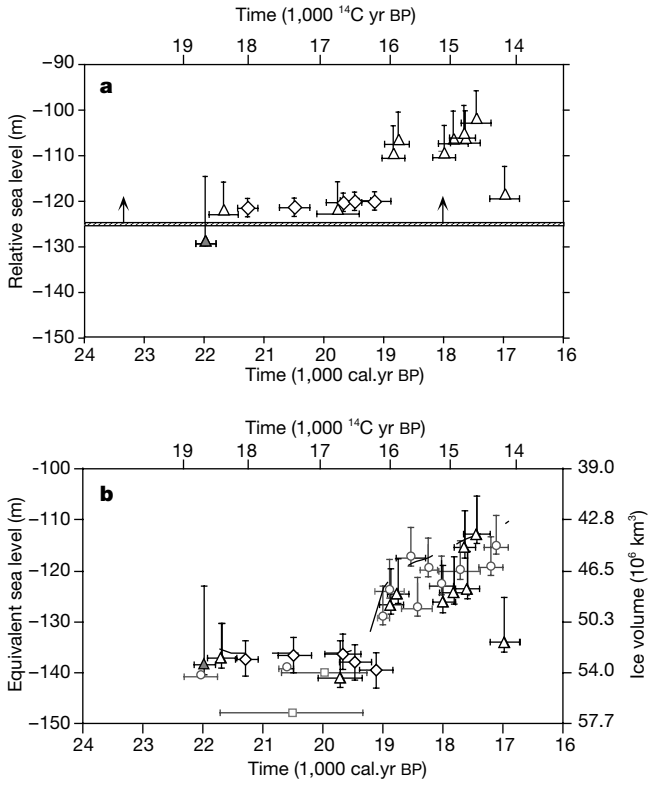

Figure 2 Sea level and ice volumes during the LGM. **a**, Observed sea level for the Bonaparte depression. The diamonds correspond to brackish-water facies, the triangles to marginal marine facies and the filed triangle to shallow marine facies. The hatched zone corresponds to the lower-limit estimate for relative sea level (according to results obtained from GC2 and 3 that neither core contains the shallow-water facies). **b**, Equivalent sea-level and ice-volume estimates. The circles correspond to the isostatically corrected Barbados data[19,20], and the squares correspond to earlier estimates for the Northwest Shelf[7]. The diamonds correspond again to brackish-water facies, the triangles to marginal marine facies, and the filled triangle to shallow marine facies. The dashed line defines the ice-equivalent sea-level function. Age uncertainties correspond to 1σ except for U/Th dated Barbados corals (2σ level)[20].

themselves. The consequence of the isostatic corrections is that the ice-volume-equivalent sea level at the LGM lies between −135 and −130 m, corresponding to a volume of grounded ice in excess of the present volume by $(52 \pm 2) \times 10^6$ km^3.

Earlier observations of the LGM sea level on the Australian shelf[7,16] and elsewhere[17,18] have shown considerable uncertainty, in part because of the limitation of the preserved indicators and in part because of inadequate age determination. Of the previous data, that of greatest importance is the Barbados evidence where the depth–age relationship of corals have placed lower limits on the local sea-level curve[19,20]. Figure 2b includes isostatically corrected sea-level estimates—using the same model and model parameters as for the Bonaparte data—for the Barbados data as well as three earlier estimates from northern Australia[7]. The main group of Barbados results, from *Acropora* corals that live in water depths down to about 5 m (ref. 19), occur in the interval from 19,000 to 17,000 cal. yr BP and, when corrected for the differential isostatic effects, are consistent with the Bonaparte Gulf data. The two older data points from Barbados lie at greater depths and are also consistent with the new data for the corresponding period. The agreement between the Barbados and Bonaparte estimates shortly after 19,000 cal. yr BP indicate that the equivalent sea level stood at about −120 m at this time, above the coral and marginal marine samples. The earlier brackish water samples occur at about −135 m equivalent sea level. These estimates are from minimally reworked fauna showing evidence of bleaching and without age inversions. Thus a rapid rise in sea level occurred at about 19,000 cal. yr BP, within a time interval defined by the dating accuracy of a few hundred years. This rapid rise was followed by a period of about 2,000 to 3,000 years of much slower melting of the ice sheets before the onset of the main phase of late-glacial melting. The bulk of the Barbados evidence, therefore, does not correspond to the period of maximum glaciation but to the early stages of the late-glacial phase.

The inferred ice-equivalent sea level of −130 to −135 m is consistent with the glaciological lower limit estimate of −127 m established by the CLIMAP project[1] and does not support the maximum CLIMAP ice-sheet reconstruction of −163 m. (It has been argued that upper- and lower-limit CLIMAP models contain excessive ice when compared with an isostatically corrected Barbados sea-level result of −105 m (ref. 21). But this latter quantity corresponds to $\Delta\zeta_{eus}$, not $\Delta\zeta_e$. A $\Delta\zeta_{eus}$ of −105 m corresponds in fact to $\Delta\zeta$ of about −135 m.)

The global sea-level observations do not indicate where the ice was stored. Analyses of sea-level data from formerly glaciated regions provide Northern Hemisphere ice volumes that are less than those contained in glaciologically based models[13,21–23] and the previously noted[14,24] discrepancy between the Northern Hemisphere and total LGM ice volumes remains. Changes in Antarctic ice may account for part of this, although estimates based on Antarctic rebound analyses are inadequate to explain the entire imbalance[25]. In the inversion of sea-level data it is the rebound within the former ice margins that is most sensitive to changes in ice volume, but the necessary observations occur only once the area becomes ice free. Hence, ice volumes for the LGM and early part of the late-glacial period remain poorly constrained in such analyses[26]. The rapid rise in sea level noted at 19,000 cal. yr BP may provide part of the answer to the missing-ice problem: that the LGM ice sheets were initially cold-based, steeply domed and thick but then, in response to basal thawing over some regions, evolved rapidly into relatively thin ice cover with a significant reduction in ice volume[27,28]. Such a hypothesis is consistent with the geomorphological field evidence[27], with glaciological modelling[29] and with the ice models inferred from rebound analyses[13,22]. □

Methods

Facies determination

To define water depth within 1–2 m in the Bonaparte Gulf, it is necessary to examine the sequence of depositional events immediately before and after the deposition of the

© 2000 Macmillan Magazines Ltd

brackish facies. In a falling sea-level sequence the following biosedimentological facies sequence can be expected within the core: 1, open marine; 2, shallow marine; 3, marginal marine; and 4, brackish conditions. The last three facies are seen, for example, in the lower part of core 5 (Fig. 1b). When sea level rises the sequence reverts to marginal marine and then to shallow marine. It is this sequence of facies changes before and after the deposition of the brackish-water sediments that determine the position and duration of shallow-water conditions. The four depositional sequences are as follows.

"Open marine" was identified by the presence of fragile pteropod remains, numerous and diversified benthic foraminifer and ostracod taxa, that are indicative of normal marine salinity. In analogy with modern conditions, water depths are around 20 m because planktonic foraminifers are either absent or rare.

"Shallow marine" was characterized by the absence of pteropods and the presence of numerous and well-preserved foraminifer and ostracod taxa (which include species of *Aglaiella*, *Argilloecia*, *Callistocythere*, *Loxoconcha*, *Pterygocythereis*, *Ulocleberis*, in addition to common bairdiid taxa); there are no planktonic foraminifers. Biodiversity of the microbiota is substantially lower than in the open marine facies. Water depths are around 10 m.

"Marginal marine" was defined by a change to a lower diversity of benthic marine ostracods (commonly encountered species: *Neocytheretta* ssp., *Xestoleberis* sp.) and benthic foraminifers, accompanied by the robust endobenthic scaphopods. Most specimens show signs of abrasion. Bivalve molluscs are common and frequently damaged. Broken echinoid spines and bryozoan remains are ubiquitous. Terrigenous material, mostly quartz, is common. Water depths are less than 5 m, being within the zone of tidal influence.

"Brackish water" was identified by a paucity of typically marine organisms and the presence of the foraminifer *Ammonia beccarii*, often in large numbers—and as dwarf morphs due to environmental stresses such as fluctuating salinities and temperatures—accompanied by the euryhaline ostracods *Cypridieis australiensis*, *Leptocythere* spp. and *Neocytheretta* spp. Signs of bleaching of the calcareous shells, indicating exposure to corrosive waters, are common. Terrigenous material is common. Salinities are well below sea-water salinity due to a strong influence of continental waters, such as found in estuaries and tidal flats. Water depths correspond to near mean sea level and up to the high-tide level. Present tidal range is ±3 m and this represents the upper limit of the accuracy of these sea-level indicators.

Received 23 July 1999; accepted 16 June 2000.

1. CLIMAP Project Members. Seasonal reconstructions of the earth's surface at the Last Glacial Maximum. *Geol. Soc. Am. Map Chart Ser.* **MC-36,** 1–18 (1981).
2. Bard, E. Ice age temperatures and geochemistry. *Science* **284,** 1133–1134 (1999).
3. Stuiver, M. & Braziunas, T. F. Modeling atmospheric ^{14}C ages of marine samples to 10,000 BC. *Radiocarbon* **35,** 137–189 (1993).
4. Edwards, R. L. *et al.* A large drop in atmospheric $^{14}C/^{12}C$ and reduced melting in the Younger Dryas, documented with ^{230}Th ages of corals. *Science* **260,** 962–968 (1993).
5. Stuiver, M. & Reimer, P. J. Extended ^{14}C data base and revised CALIB 3.0 ^{14}C age calibration program. *Radiocarbon* **35,** 215–230 (1993).
6. Bard, E., Arnold, M., Hamelin, B., Tisnerat-Laborde, N. & Cabioch, G. Radiocarbon calibration by means of mass spectrometric $^{230}Th/^{234}U$ and ^{14}C ages of corals. An updated data base including samples from Barbados, Mururoa, and Tahiti. *Radiocarbon* **40,** 1085–1092 (1998).
7. van Andel, T. H., Heath, G. R., Moore, T. C. & McGeary, D. F. R. Late Quaternary history, climate, and oceanography of the Timor sea, Northwestern Australia. *Am. J. Sci.* **265,** 737–758 (1967).
8. De Decker, P. An account of the techniques using ostracods in palaeolimnology in Australia. *Palaeogeogr. Palaeoclimat. Palaeoecol.* **62,** 463–475 (1988).
9. Yassini, I. & Jones, B. G. (eds) *Recent Foraminifera and Ostracoda from Estuarine and Shelf Environments on the Southeastern Coast of Australia* (Univ. Wollongong Press, 1995).
10. Farrell, W. E. & Clark, J. A. On postglacial sealevel. *Geophys. J.* **46,** 79–116 (1976).
11. Nakada, M. & Lambeck, K. Glacial rebound and relative sea-level variations: a new appraisal. *Geophys. J. R. Astron. Soc.* **90,** 171–224 (1987).
12. Lambeck, K. & Nakada, M. Late Pleistocene and Holocene sea-level change along the Australian coast. *Palaeoceogr. Palaeoclimatol. Palaeoecol.* **89,** 143–176 (1990).
13. Lambeck, K., Smith, C. & Johnston, P. Sea-level change, glacial rebound and mantle viscosity for northern Europe. *Geophys. J. Int.* **134,** 102–144 (1998).
14. Nakada, M. & Lambeck, K. The melting history of the Late Pleistocene Antarctic ice sheet. *Nature* **33,** 36–40 (1988).
15. Fleming, K. *et al.* Refining the eustatic sea-level curve since the Last Glacial Maximum using far- and intermediate-field sites. *Earth Planet. Sci. Lett.* **163,** 327–342 (1998).
16. Ferland, M. A., Roy, P. S. & Murray–Wallace, C. V. Glacial lowstand deposits on the outer continental shelf of southeastern Australia. *Quat. Res.* **44,** 294–299 (1995).
17. Ota, Y., Matsushima, Y. & Moriwaki, H. Notes on the Holocene sea-level study in Japan. *Quat. Res. Jpn* **21,** 133–143 (1982).
18. Colonna, M., Casanova, J., Dullo, W.-C. & Camoin, G. Sea-level changes and $\delta^{18}O$ record for the past 34,000 yr from Mayotte Reef, Indian Ocean. *Quat. Res.* **46,** 335–339 (1996).
19. Fairbanks, R. G. A 17,000-year glacio-eustatic sea level record: influence of glacial melting rates on the Younger Dryas event and deep-ocean circulation. *Nature* **342,** 637–642 (1989).
20. Bard, E., Hamelin, B. & Fairbanks, R. G. UpTh ages obtained by mass spectrometry in corals from Barbados: sea level during the past 130,000 years. *Nature* **346,** 456–458 (1990).
21. Peltier, W. R. Ice age paleotopography. *Science* **265,** 195–201 (1994).
22. Tushingham, A. M. & Peltier, R. W. Ice-3G: A new global model of late Pleistocene deglaciation based upon geophysical predictions of post-glacial relative sea level change. *J. Geophys. Res.* **96,** 4497–4523 (1991).
23. Lambeck, K. Limits on the areal extent of the Barents Sea ice sheet in Late Weichselian time. *Glob. Planet. Change* **12,** 41–51 (1996).
24. Andrews, J. T. A case of missing water. *Nature* **358,** 281 (1992).
25. Zwartz, D., Lambeck, K., Bird, M. & Stone, J. in *The Antarctic Region: Geological Evolution and Processes* (ed. Ricci, C. A.) 821–828 (Terra Antarctica, Siena, 1997).
26. Johnston, P. & Lambeck, K. Automatic inference of ice models from postglacial sea-level observations: Theory and application to the British Isles. *J. Geophys. Res.* 13179–13194 (2000).
27. Kleman, J. & Hättestrand, C. Frozen-bed Fennoscandian and Laurentide ice sheets during the Last Glacial Maximum. *Nature* **402,** 63–66 (1999).
28. Clark, P. U., Alley, R. B. & Pollard, D. Northern hemisphere ice-sheet influences on global climate change. *Science* **286,** 1104–1111 (1999).
29. Licciardi, J. M., Clark, P. U., Jenson, J. W. & Macayeal, D. R. Deglaciation of a soft-bedded Laurentide ice sheet. *Quat. Sci. Rev.* **17,** 427–448 (1998).

Acknowledgements

We thank J. Marshall for providing access to cores collected by the Australian Geological Survey Organisation.

Correspondence and requests for materials should be addressed to K.L. (e-mail: Kurt.Lambeck@anu.edu.au).

Cursoriality in bipedal archosaurs

Terry D. Jones*†, James O. Farlow‡, John A. Ruben*, Donald M. Henderson§ & Willem J. Hillenius‖

* *Zoology Department, Oregon State University, Corvallis, Oregon 97331, USA*
‡ *Department of Geosciences, Indiana-Purdue University, Fort Wayne, Indiana 46805, USA*
§ *Department of Cell Biology and Anatomy, School of Medicine, The Johns Hopkins University, Baltimore, Maryland 21205, USA*
‖ *Biology Department, College of Charleston, Charleston, South Carolina 29424, USA*

Modern birds have markedly foreshortened tails and their body mass is centred anteriorly, near the wings[1–5]. To provide stability during powered flight, the avian centre of mass is far from the pelvis, which poses potential balance problems for cursorial birds. To compensate, avians adapted to running maintain the femur subhorizontally, with its distal end situated anteriorly, close to the animal's centre of mass; stride generation stems largely from parasagittal rotation of the lower leg about the knee joint[6–12]. In contrast, bipedal dinosaurs had a centre of mass near the hip joint and rotated the entire hindlimb during stride generation[4–8,11–13]. Here we show that these contrasting styles of cursoriality are tightly linked to longer relative total hindlimb length in cursorial birds than in bipedal dinosaurs. Surprisingly, *Caudipteryx*, described as a theropod dinosaur[14,15], possessed an anterior centre of mass and hindlimb proportions resembling those of cursorial birds. Accordingly, *Caudipteryx* probably used a running mechanism more similar to that of modern cursorial birds than to that of all other bipedal dinosaurs. These observations provide valuable clues about cursoriality in *Caudipteryx*, but may also have implications for interpreting the locomotory status of its ancestors.

In contrast to bipedal dinosaurs, the femur in cursorial birds contributes little to generation of stride length, and avian hindlimb movement is largely the result of retraction of the lower leg[7–12]. Hence, it might be expected that relative stride length in cursorial birds would be lower than that in bipedal dinosaurs. However, this is probably not the case—lengths of 'effective hindlimb' segments in birds (tibiotarsus + tarsometarsus) and dinosaurs (femur + tibia + metatarsal III) are equivalent[16] (Fig. 1a). Consequently, total hindlimb length in cursorial birds is invariably one-and-a-half times longer than in theropod and ornithopod dinosaurs (Fig. 1b). Additionally, as adept avian runners have evolved repeatedly from flighted ancestors[17], we conclude that these profound anatomical modifications that facilitate avian cursoriality are multiple convergent responses to secondary resumption of cursoriality in distantly related taxa independently derived from flighted ancestors.

† Present address: Department of Biology, Stephen F. Austin State University, Nachogdoches, Texas 75962, USA.

© 2000 Macmillan Magazines Ltd